Design and assessments on a hybrid pin fin-metal foam structure towards enhancing melting heat transfer

An experimental study

Liu, Gang; Du, Zhao; Xiao, Tian; Guo, Junfei; Lu, Liu; Yang, Xiaohu; Hooman, Kamel

DOI
10.1016/j.ijthermalsci.2022.107809

Publication date
2022

Document Version
Final published version

Published in
International Journal of Thermal Sciences

Citation (APA)
Liu, G., Du, Z., Xiao, T., Guo, J., Lu, L., Yang, X., & Hooman, K. (2022). Design and assessments on a hybrid pin fin-metal foam structure towards enhancing melting heat transfer: An experimental study. *International Journal of Thermal Sciences*, *182*, Article 107809. https://doi.org/10.1016/j.ijthermalsci.2022.107809

International Journal of Thermal Sciences 182 (2022) 107809

Contents lists available at ScienceDirect

International Journal of Thermal Sciences

journal homepage: www.elsevier.com/locate/ijts

Design and assessments on a hybrid pin fin-metal foam structure towards enhancing melting heat transfer: An experimental study

Gang Liu [a,1], Zhao Du [a,1], Tian Xiao [b], Junfei Guo [a], Liu Lu [a], Xiaohu Yang [a,*], Kamel Hooman [c]

[a] Institute of the Building Environment & Sustainability Technology, School of Human Settlements and Civil Engineering, Xi'an Jiaotong University, Xi'an, 710049, China
[b] State Key Laboratory for Strength and Vibration of Mechanical Structures, School of Aerospace, Xi'an Jiaotong University, Xi'an, 710049, PR China
[c] Process & Energy Department of the 3mE Faculty, Delft University of Technology, Delft, the Netherlands

ARTICLE INFO

Keywords:
Solar energy
Phase change heat storage
Fin-copper foam composite
Experimental measurement

ABSTRACT

Solar energy, as a kind of renewable energy, offers a large reserve to be harvested at a reasonably low cost for engineering applications. To decouple the temporal and spatial relevance of the continuous energy supply of solar energy, latent heat thermal energy storage can deal with this problem at different temperatures. Aiming to improve energy efficiency, a novel hybrid metal foam-pin fin structure is designed and assessed. Upon conducting measurements on a well-designed experimental bench, the phase change processes of paraffin that is filled in fins, metal foam, and a combination of both (hybrid structure) are evaluated. During the experiments, the transient melting interface is snapshotted and temperature development is documented under five different heat source temperatures of 61 °C, 63 °C, 65 °C, 68 °C, and 70 °C. In the foreground of the novel hybrid structure, each segment of the hybrid is also justified and discussed. Results indicate that the hybrid structure augments marked heat transfer. Compared to pure PCM, complete melting time decreases by 63.4% and simultaneously the temperature response rate increases by 143.9% as implementing the hybrid. Attempts to design hybrid structure find a solution to assess and operate thermal storage applications for solar engineering.

1. Introduction

As a kind of renewable energy, solar energy has been addressing the vital interests owing to its clean, large reserves and pollution-free characteristics [1]. Solar energy offers a large reserve to be harvested at a reasonably low cost for engineering applications. Intermittent problem of solar energy, however, mandates the need to store energy. Thermal energy storage (TES) offers to store heat at different temperatures either for direct use or its conversion to another form of energy like electricity [2]. For such systems, the latent heat absorbed in the phase change material (PCM) is often used for heat storage at a relatively constant temperature [3,4]. The application and development prospects of PCMs in different solar systems include solar thermal power plants [5,6], solar water heaters [7,8], solar air heaters [9,10], and building heating and cooling sector [11,12]. Paraffin wax, as a typical organic solid-liquid PCM, offers good stability, no corrosiveness and supercooling, high latent heat density, and small density variation during phase change. However, its low thermal conductivity is a vital reason for its slow charging and discharging efficiency. Therefore, a number of techniques are implemented to increase the thermal conductivity, for instance by using triplex tubes [13,14], fins [15,16], microencapsulation [17,18], nanoparticles [17,18], packed bed [19,20], metal foam [21,22], graphite foams [23,24], heat pipes [25] and thermal siphons [26].

In various methods to enhance heat transfer, metal foam is one of them worthy of attention. The experimental tests found that the open-cell metal foam has a superior heat transfer enhancement effect on PCM [27,28]. The main reason is that the open-cell metal foam has a large specific surface area and high thermal conductivity metal skeleton. Hu et al. [29] measured the temperature field of PCM inside aluminum foam with low porosity. Both the melting and the temperature uniformity were enhanced. It was recommended that a more uniform temperature distribution (improved by 83.3%) was achieved inside PCM-foam block than the PCM. Huang et al. [30] experimentally observed the melting behaviors in paraffin filled copper foam. The documented melting front indicated that the phase interface was not smooth at mesoporous scale. Al-Jethelah et al. [31] explored the influences of nanoparticle-enhanced PCM and metal foam on the melting process. They recommended that adding nanoparticles to metal foam

* Corresponding author.
E-mail address: xiaohuyang@xjtu.edu.cn (X. Yang).
[1] The first two authors contributed equally to this paper.

https://doi.org/10.1016/j.ijthermalsci.2022.107809
Received 4 February 2022; Received in revised form 15 June 2022; Accepted 14 July 2022
Available online 3 August 2022

Nomenclature

Abbreviation

LTES	Latent thermal energy storage
MEPCM	Microencapsulated phase change material
PCMs	Phase change materials
PCM	Phase change material
PID	Proportion Integration Differentiation
TES	Thermal energy storage

Symbols

RR	Temperature response rate
T	Temperature (℃)
T_{wall}	Wall temperature (℃)
T_{base}	Base plate temperature (℃)
$T_{thickness}$	Thickness directional temperature (℃)
T_{fin}	Fin temperature (℃)
T_{height}	Height directional temperature (℃)
t	Time (s)
t_{total}	Complete melting time (s)
δT	Measurement uncertainty
δT_a	Thermocouple in the temperature range of permissible error
δT_b	Thermocouple compensating conductor error
δT_c	Instrumentation error

Table 1
Physical property.

Property	Density / kg•m^{-3}	Thermal conductivity / W·m^{-1}·K^{-1}	Specific heat capacity / J·kg^{-1}·K^{-1}	Latent heat / kJ·kg^{-1}
Copper	8978	381	387.6	None
Paraffin	800	0.2 (solid) / 0.1 (liquid)	2000	102

Table 2
Uncertainty in the testing bench system.

Source of uncertainty	Value/°C
δT_a	±0.2
δT_b	±0.15
δT_c	±0.1

positively affected the melting process and can accelerate the heat storage rate. Marri and Balaji [32] measured the melting improvement of metal foam. They claimed that the performance was achieved 4.4 times higher than the original PCM. Besides, they also optimized the porosity distribution and obtained another 28% improvement compared with the uniform foam. Li et al. [33] built a test bench to examine the melting procedure of PCM with copper foam. A series of experimental observations are made under different foam parameters. The partial configuration on metal foam porosity decreased the melting time by 8.03% using the same foam mass.

The experimental explorations of the characteristics of the foam composite PCM are limited by experimental conditions. Numerical simulation can supplement the experiment to understand the heat transfer mechanism better. The volume average method represents metal foam in the fluid properties of composite materials, and the physical properties are displayed on a macro scale, which reduces the calculation time and maintains actual properties. Moussa et al. [34]

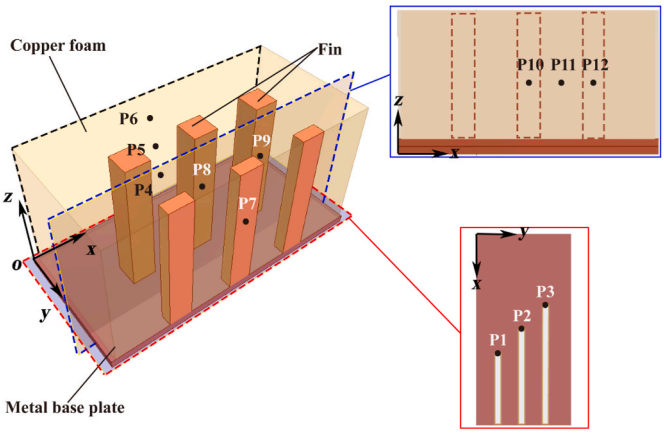

Fig. 1. Sketch of the fin-foam sample (half) and positions for the thermocouples.

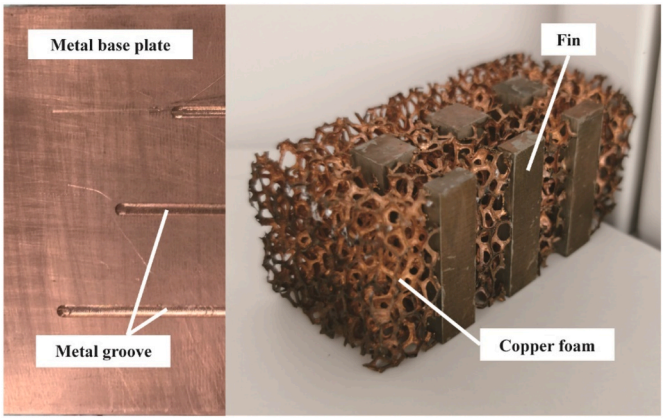

Fig. 2. Fin-metal foam sample and the grooves for holding thermocouples.

attempted to simulate the melting of porous media with distinctive porosities. Two-temperature equation models and local non-thermal equilibrium assumptions accounted for the interstitial heat transfer between PCM and the metallic framework. Joshi and Rathod [35] further studied the metal foam-paraffin composite and compared numerical simulation with experimental results to find the applicability of the two-temperature equation models. Melting characteristics under different filling ratios were numerically tested. Results revealed that the partially-filling pattern had better improvement. Buonomo et al. [36] used Darcy-Fochheimer's law and local thermal equilibrium model to numerically describe the heat transfer between metal foam and PCM. Guo et al. [37] attempted to investigate the influences of compression upon melting of paraffin-foam hybrid. Compared with uncompressed foam, observations revealed that compression had a predominated effect on melting, at a reduction rate of 13.9% in melting time. Except for volume average method, pore-scale simulation [38] and Lattice Boltzmann method [39] have also been employed for simulation. Wang et al. [40] simulated the heat transfer in composite PCM at pore scale and found that the foam pore size exerted limited contribution to heat transfer, while the porosity affected the thermal conductivity of the composite profoundly. Besides, the phase interface was affected by the metal foam microstructure. Abishek et al. [41] investigated the microscopic properties of PCM saturated in aluminum foam. Pores, framework, specific surface, and pore size were examined. An empirical relationship of the dimensionless specific surface area was proposed. Results documented that the specific surface dominated the melting rate. Ferfera et al. [42] justified the influences of porosity upon composite PCM at pore scale, and found that a decrease in porosity would

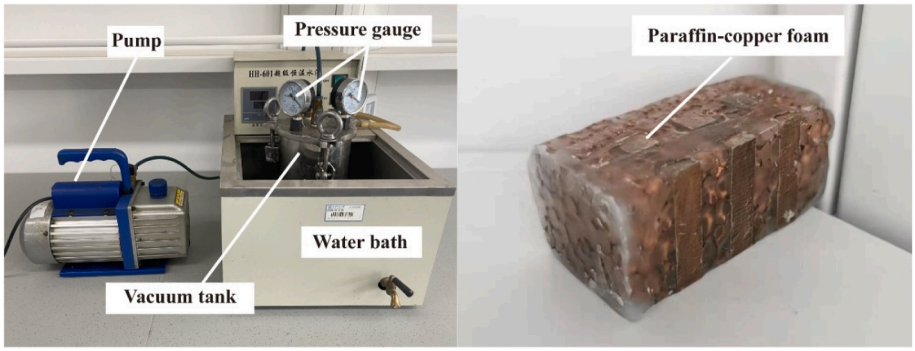

Fig. 3. Paraffin-copper foam vacuum infusion and the prepared sample.

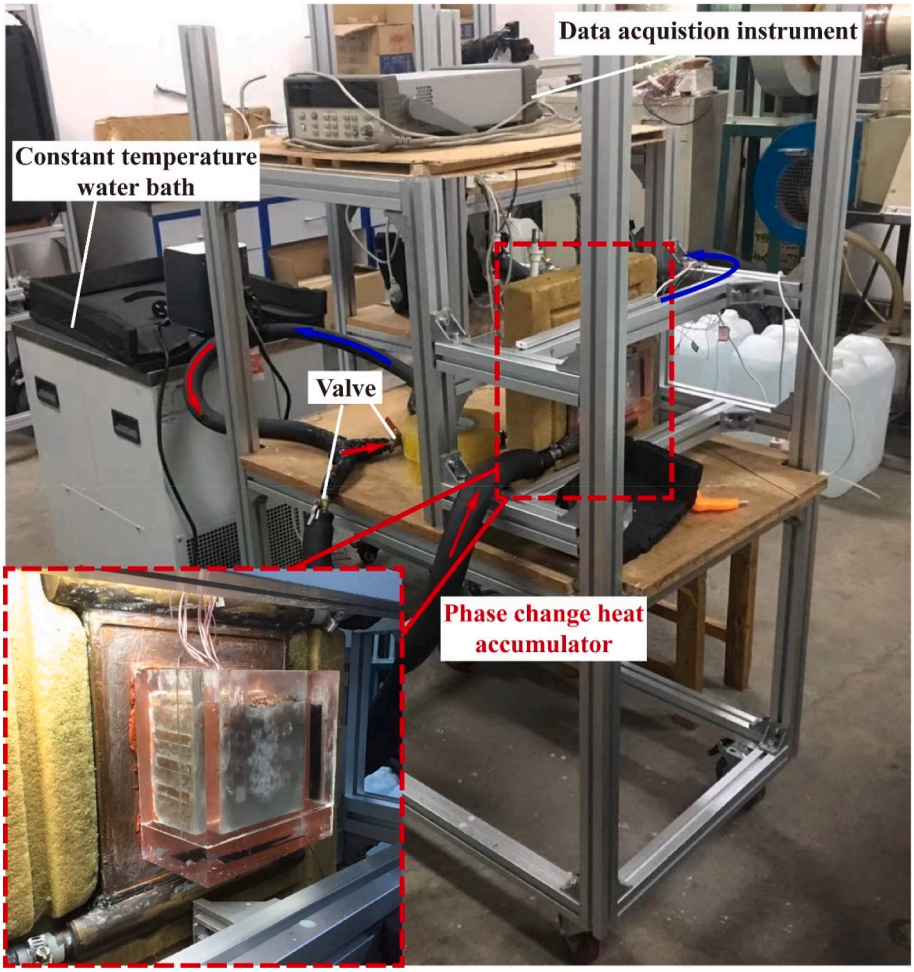

Fig. 4. Phase change heat exchanger testing system.

result in faster heat diffusion in PCM and an increase in thermal conductivity. Gaedtke et al. [43] and He et al. [44] elaborated on the Lattice Boltzmann method and its applications with the solid-liquid phase change in porous structures, which is suitable for simulating thermo-fluidic models on more complex boundaries. Pore-scale simulation and Lattice Boltzmann method focus on the microscopic characteristics of the metal foam, which can better reflect the internal characteristics, but require more calculation time.

As an alternative, fins have also been used to serve the same purpose, that is, to enhance the conductivity leading to faster charge and discharge. Xu et al. [45] replaced a pure paraffin tank with the one filled by three layers of paraffin with different melting temperatures. Compared with the pure PCM, adding fins effectively saves up to 71% of melting time. Yıldız et al. [46] investigated the interplay between the fins and natural convection when the PCM melted into liquid. Besides, Fekadu and Assaye [47] justified the influence of fin parameters on the melting process in a rectangular shell under adiabatic conditions. De Césaro Oliveski et al. [48] studied the effect of changing area fraction and aspect ratio on the melting process in a rectangular cavity with single fin. To further improve the phase change performance, conventional fins are innovated with various shapes. Compared with uniform fins, the bifurcated fin [49], rectangular and triangular combined fins [50], and gradient tree-shaped fins [51] could enhance the heat transfer and shorten the charging time. The fin number, spiral period, and

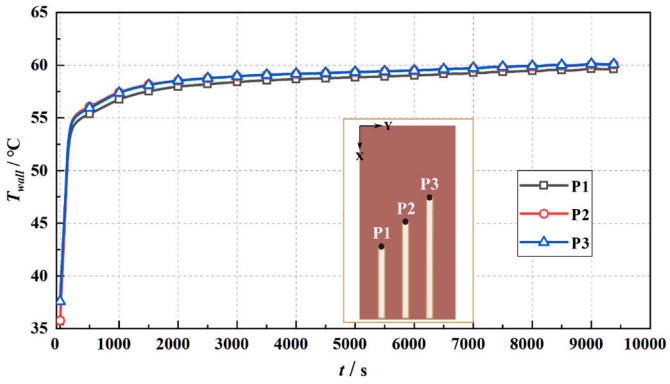

Fig. 5. Wall temperatures at three selected points under a heat source temperature of 61 °C.

thickness are key parameters that affect the thermal storage performance in the spiral fin [52]. In addition, Deng et al. [53] designed the fern fractal fin structure according to the bionic principle and optimized the parameters. Compared with the straight fin, the average heat storage rate of the fractal fin was increased by 88.3%. Previous studies demonstrated that the innovated fins were more efficient than the conventional rectangular fins.

Except for the design on fin shapes to improve the melting phase change, the inclusion of enhancers, including porous foam [54,55] and nanomaterials [56], can further accelerate melting since the conductivity enhancers markedly increase the thermal conductivity of PCM in a more uniform fashion. The heat storage/release performance of annular fin-metal foam [57] and plate fin-metal foam structure [58] were analyzed by numerical simulation. The results showed that the new structure could strengthen the solidification process better than the melting process. Yang et al. [59] calculated the phase transition efficiency of gradient metal foams on the solidification process in pin fin foam structure. Chen et al. [60] studied parameters of finned metal foam structure under different super-gravity conditions. Meng et al. [61] changed the shape of the plate fins in the copper foam structure with fins, and observed the thermal performance of seven trapezoidal fins. The above research had only focused on numerical simulation. Besides, previous studies lack experimental testing of structures over the common temperature range of solar energy utilization or other low-temperature heat sources. However, these results not only need to be verified experimentally, but the experiments can better reflect the actual heat storage performance and heat loss.

While either the foams and fins are extensively studied in the literature, there are only relatively few studies that combine the benefits of both metal foams and fins in existing numerical investigations. In general, most of them focus on how various parameters of plate/annular fins affect the melting/solidification process. The experimental results are relatively few, and sometimes the plate fin cannot produce a more uniform heat transfer than the pin fin. Compared with previous structures, pin fins can theoretically take up less volume to strengthen the local heat transfer, thereby improving the overall heat storage and release efficiency. Therefore, this paper addresses manufacturing a hybrid pin fin-foam structure, which is then tested under different operating conditions in a well-designed test bench system. To assess the benefits of this new design, tests are also conducted for pure paraffin as well as two other designs one with fins and the other one with metal foams.

2. Experimental bench system

2.1. Fin-foam hybrid structure

The main materials used in the construction of the four structures in this paper are paraffin, copper and copper foam. The physical properties of copper and paraffin are listed in Table 1. Copper foam that is used for this test is characterized using its porosity (0.97) and pore density (10 PPI, pore per inch). The foam is a rectangular parallelepiped block of 68 mm × 34 mm × 30 mm in size. There are totally 12 pin fins of square cross section inserted in the foam block, and half of the sample is presented in Fig. 1. The fins are set horizontally in-line 7 mm apart where gravity pulls in the positive *X* direction for arrangement in experiments. A 4-mm-thick copper base plate separates the fin-foam compound from the heat source. The pin fin size is 6 mm × 6 mm × 30 mm. Thermal conductive silver adhesive (Arctic Silver-Premium Silver Thermal Cooling Adhesive) is used to glue the fin-foam hybrid structure itself and to the copper base plate. The high conductivity of the copper plate is expected to result in a uniform temperature distribution over the plate. The base plate temperature uniformity is verified using three thermocouples inserted in 2-mm-diameter grooves drilled to 39 mm, 34 mm, and 29 mm depth as shown in Fig. 2 (denoted by P1–P3). A total of 12 T-type thermocouples with a diameter of 2 × 0.255 mm are arranged inside the copper foam specimen, with a temperature measurement range of −200 °C ~ 260 °C. In Fig. 2, three thermocouples are arranged in the thickness direction (the positive *Z* axis), the height direction (the positive *X* axis), and the fins, in respective.

The vacuum infusion technique is used to ensure the PCM infiltration in the hybrid fin-foam sample, as shown in Fig. 3. The air inside metal foam will bring greater resistance to filling PCM in the air. In addition, filling PCM directly may result in bubbles forming inside the PCM. However, the vacuum infusion technique can pre-emptive evacuation the air inside the metal foam to avoid these problems. Therefore, the vacuum infusion is selected in this study. The hybrid foam-fin structure is placed in a vacuum tank which is then filled with solid paraffin. A vacuum pump brings the gauge pressure down to 0.01 MPa while the vacuum tank is immersed in the water bath and kept at 100 °C for 2 h. Upon these processes, the PCM is then completely melted. Subsequently, the vacuum tank is pulled out and left to cool down to room temperature to ensure that the PCM is completely solidified. Excessive parts of the paraffin layer, as shown in Fig. 3, is then removed so that the sample can set in the test section.

2.2. Experimental system

A well-designed experimental bench system allowing melting phase change test is designed and assembled in Fig. 4. The experimental bench is designed into three parts: the thermal fluid circulation part, the phase change test part, and the real-time data acquisition part.

The constant temperature water bath, heat transfer fluid (HTF), ball valve, and plastic hose form the thermal fluid circulation part. The HTF temperature is controlled by the constant temperature water bath, and the HTF (deionized water) is sent into the plastic hose through the built-in circulating pump. At this time, the internal and external circulation can be regulated by the valves for first internal circulation to make the HTF reach a predetermined temperature and then for the outer circulation to carry out phase change tests. The constant temperature water bath used in the experiment is the CORIO CD-1001 F universal heating and refrigeration circulator produced by JULABO. A 2-kW heating and cooling unit is incorporated inside the circulator water bath. The operating temperature range is −38°C ~ 100 °C. It is controlled by Proportion Integration Differentiation (PID) with temperature stability of ±0.03 °C.

For the melting test part, a rectangle Plexiglas tank is fabricated to house the fin-foam hybrid to allow for visual access. A microchannel heat exchanger that is embedded in the polyurethane foam serves as the bottom for the Plexiglas tank (see the enlargement in Fig. 4). The hybrid specimen is placed in the center of the micro-channel heat exchanger, in which the heat-conducting silicone grease is uniformly smeared to reduce the heat transfer resistance. A 5 mm height chamber is reserved on the upper part of the Plexiglas tank to allow for volume expansion of

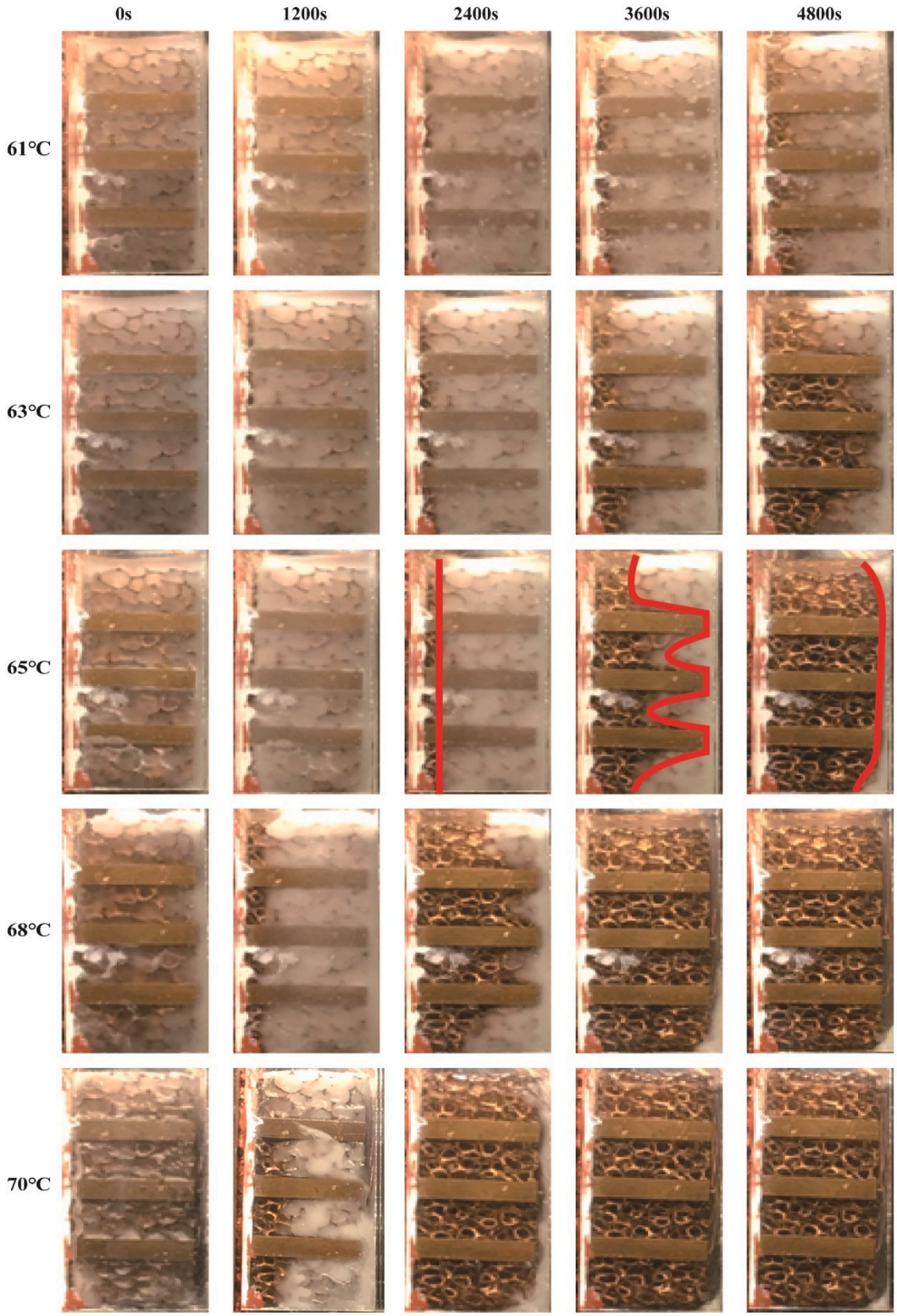

Fig. 6. Phase interface change under different heat source temperatures.

PCM. An insulation cotton covers the whole Plexiglas tank to reduce heat losses.

The real-time data acquisition part is composed of collector, camera, computer, and accessories. A data acquisition system (KEYSIGHT, model 34970 A) is devised. A camera is setup on one side of the tank to take pictures (at a fixed interval of 5 min) and record the interface movement during melting. BenchLink Data Logger software of KEYSIGHT provides real-time Data display and storage analysis for the temperature measurement.

2.3. Experimental measurement uncertainty

In this experiment, the main targeted variable is temperature in the process of melting, using T-type thermocouple and Agilent data collector

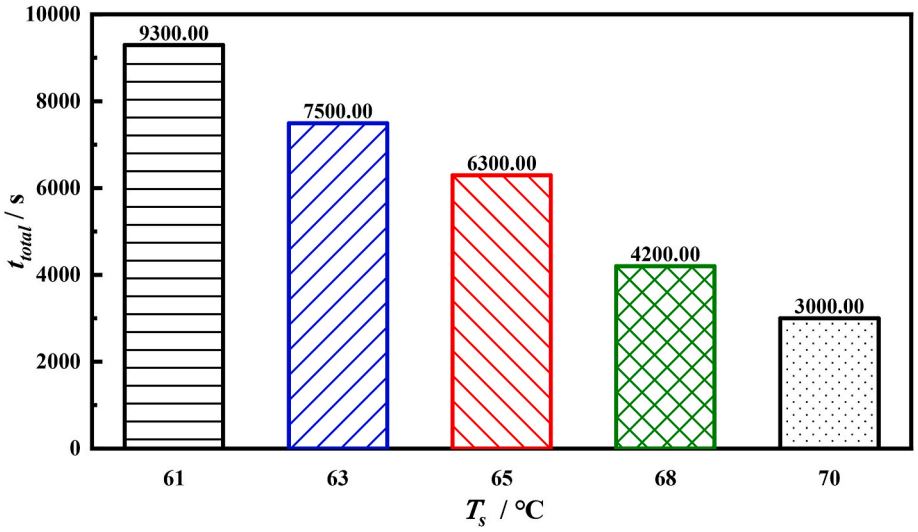

Fig. 7. Complete melting time under different heating temperatures.

(Agilent 34970a) for data collection. Occurring in the process of measurement uncertainty (δT) includes thermocouples in the temperature range of permissible error (δT_a), thermocouple compensating conductor error (δT_b), and the instrumentation error of acquisition instrument (δT_c). The uncertainty in the testing bench system is listed in Table 2. To sum up, the temperature uncertainty in this experiment is:

$$\delta T = \sqrt{(\delta T_a)^2 + (\delta T_b)^2 + (\delta T_c)^2} = 0.27^{\circ}\mathrm{C} \quad (1)$$

The final measurement uncertainty for temperature (0.27 °C) can meet the experimental requirements, indicating the high reliability of experimental data. The errors are demonstrated in.

3. Results and discussions

Here we first compare the new design to the existing heat transfer augmentation techniques and, of course, all cases will be compared against pure PCM melting as a benchmark case. Then we move on to presenting the characteristics for the hybrid fin-foam case.

3.1. Substrate wall temperature (T_{wall})

Five source temperatures of 61 °C, 63 °C, 65 °C, 68 °C, and 70 °C are guaranteed for thermal storage. Here, the case with source temperature of 61 °C is displayed. As for the wall temperature, the measurement points are displayed in Fig. 5. The three points P1, P2, and P3 are 39 mm, 34 mm, and 29 mm away from the origin in the *X* direction, and the left and right distances between the three are 5 mm in the *Y* direction, in respective. As seen, the three thermocouples record very close readings (within 0.36 °C). This reassures the anticipated base plate temperature uniformity. It should be mentioned here that the temperatures of the three are finally stabilized at 59.9 °C, lower than the heat source (water tank) temperature of 61 °C, owing mainly to the heat losses from the circulating pipes and valves.

3.2. Melting front evolution

Tests are conducted for five values of heat source temperatures being 61 °C, 63 °C, 65 °C, 68 °C, and 70 °C. As illustrated by Fig. 6, successive images taken by the camera allow for heat transfer and flow visualization, favoring the conclusion that heating temperature has a significant improvement on melting process. As seen, with three lower heat source temperatures, i.e., 61 °C, 63 °C and 65 °C, there is no sign of melting the paraffin wax during the first 1200 s of the tests. The heat is obviously stored in the compound and increases the PCM (sensible heat) temperature; yet below the melting point. A melting front is noted with time, which then moves away from the heated surfaces. As expected, melting starts from the heated wall (the left side in the figure is the heating side). The melting front appears as a vertical line initially. With time elapsing, the melting front follows fin patterns. This can be explained as fins offer lower conduction resistance compared with PCM-filled pores of the foam. Interestingly, the presence of the fin and foams minimizes the shrinking stage which, in the absence of thermal conductivity enhancer, i.e., with pure PCM, can significantly prolong the melting process. The images indicate that heat is mainly conducted and that the contribution of convective heat transfer is comparably insignificant. This interesting observation can significantly help numerical simulation of such systems where the convective terms can be dropped and a conduction heat transfer problem can lead to accurate (enough) results.

3.3. Complete melting time

For a TES design, the time required to charge the system fully is of great importance. As shown in Fig. 7, the time to fully melt the PCM is 9300 s, 7500 s, 6300 s, 4200 s, and 3000 s when the heat source temperature is 61 °C, 63 °C, 65 °C, 68 °C, and 70 °C, respectively. In the range of 61 °C ~ 68 °C, for every 1 °C increase in heat source temperature, the total melting time will decrease by 700 s on average. While at 70 °C, the heat source temperature will increase by 2 °C compared with 68 °C, and the complete melting time will decrease by 1200 s. With the heat source temperature increasing, the average reduction in complete melting time at 61 °C ~ 68 °C is greater than the average reduction in complete melting time at 68 °C ~ 70 °C, indicating that simply increasing the heat source temperature capably reduces the melting time. Nevertheless, increasing heat source temperature in the high temperature region does not lead to better desired heat transfer improvement. Therefore, it is necessary to find the most suitable heat source temperature.

3.4. Comparison among four different structures

3.4.1. Comparison of phase interface

Fig. 8 is presented to visually compare the melting process of pure PCM with three other techniques used here for heat transfer augmentation. Four images are taken for each scenario, and for all cases, the heat source temperature is set at 70 °C. A quick visual inspection shows that the hybrid design outperforms the other three cases. Much faster melting and less shrinkage compared with the other three cases favor the

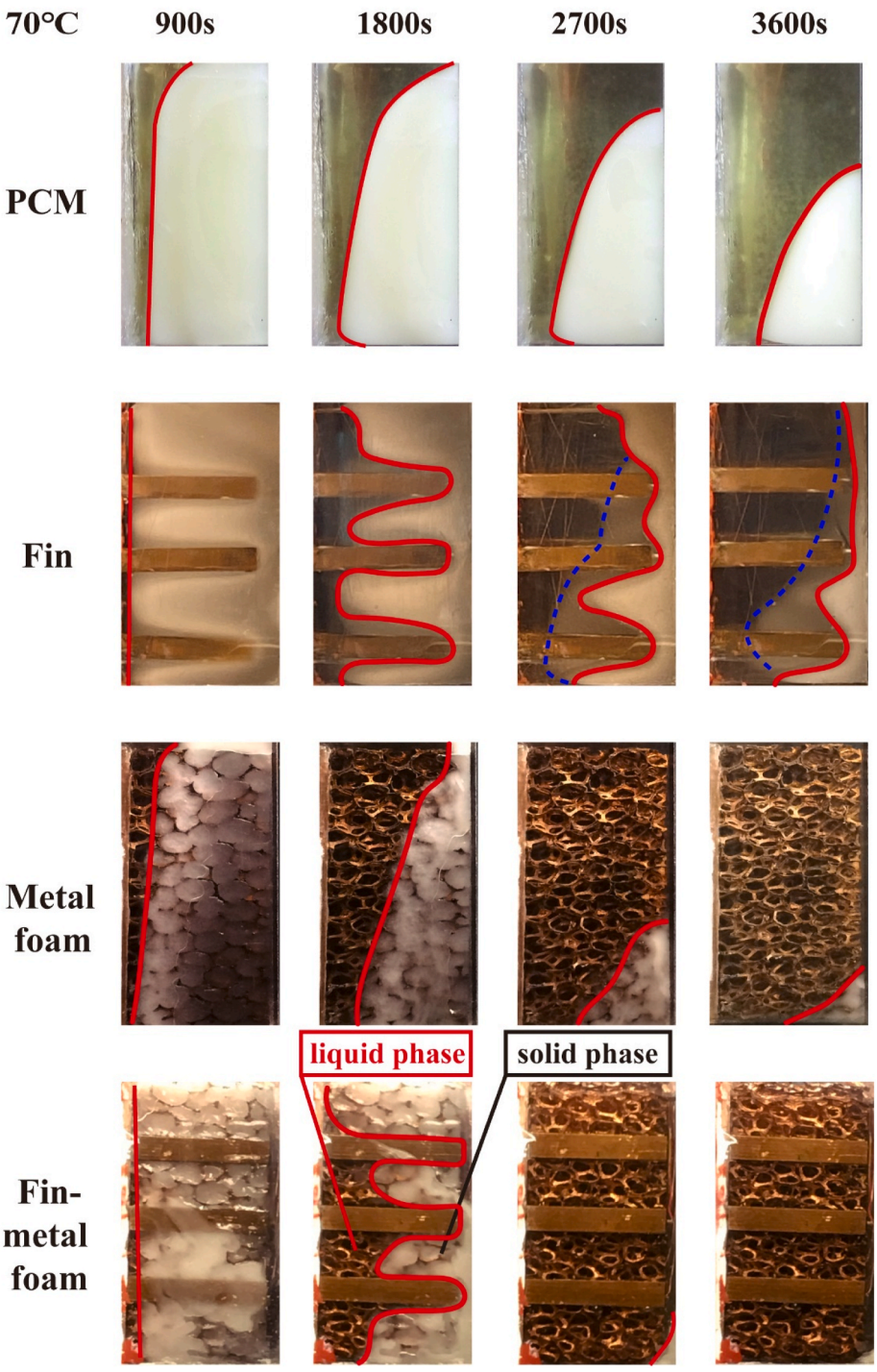

Fig. 8. Comparison of phase interface in four structures under a heat source temperature of 70 °C.

choice of the hybrid design.

Starting with the image taken at 900 s, all four cases demonstrate a thin near-wall liquid layer. Moving on 1800 s, all designs, except for the hybrid one, show some degree of free convection heat transfer. Pure paraffin clearly follows the four-stage phase change process described in Jany and Bejan [62]. The design with metal foam shows free convection effects as the interface is not a perfectly vertical line to demonstrate the influence of free convection upon forming interface shape and location. As one would expect, a 3D buoyancy-induced flow is observed with pin-fins. This can be attributed to different melting rates in plane between the fins compared with a plane away from the fins. A faster melting rate at the fin leads to a higher liquid fraction in the vicinity of the fins (red line) compared with regions away from the fin (blue line). With time, the liquid is overheated while the solid phase temperature is limited (lower than the melting point). This local difference derives a buoyancy-induced flow which is more noticeable in the image taken after 2700 s. One notes two different shades of the solid fraction; the one is closer to the light source instead of the darker shade of the solid phase, which obviously demonstrates a slower melting rate away from the fins. To better convey the point, we use blue dashed lines to show the interface captured on two different planes. The red solid line shows the interface over a plane containing fins while the blue dashed line clearly shows the melting front at a parallel plane that crosses no fins. At the same time, in the fin-foam case, thanks to the composite improving

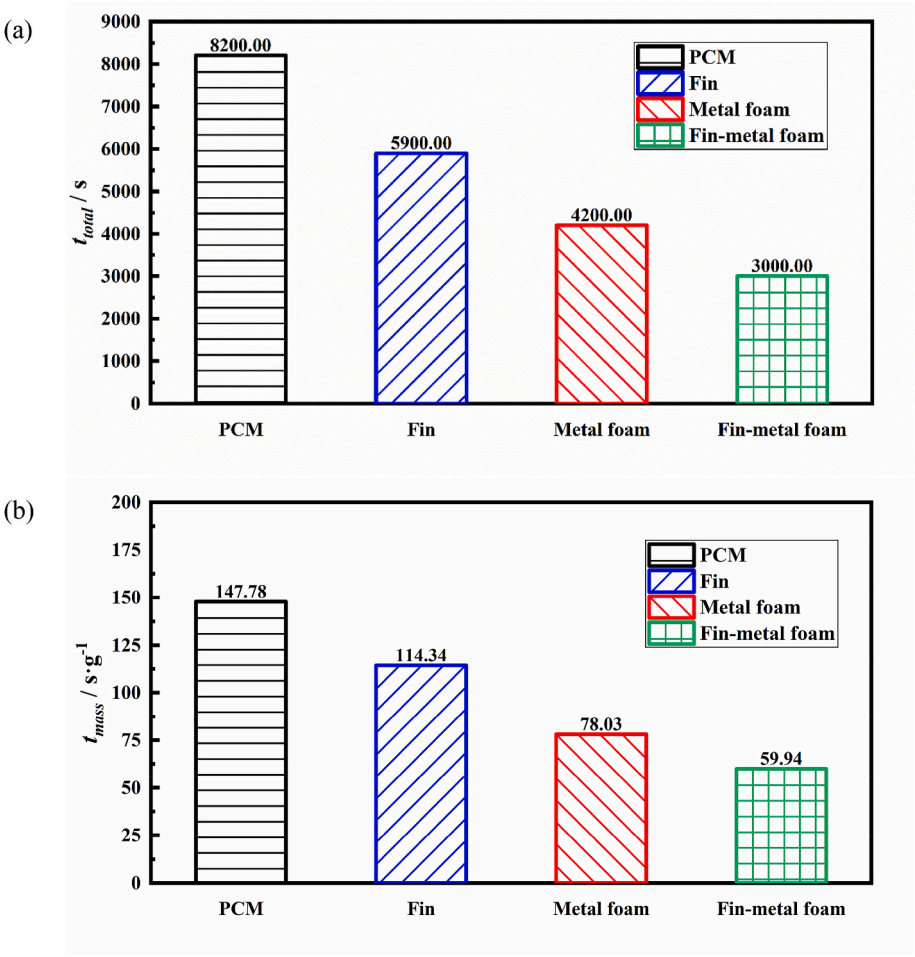

Fig. 9. Comparison of (a) total melting time and (b) melting time per unit PCM mass.

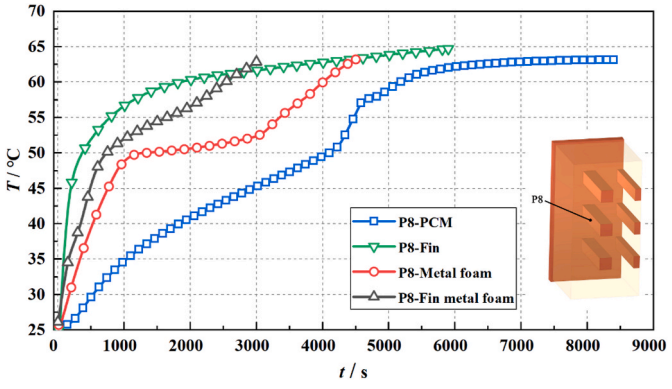

Fig. 10. Comparison of temperature changes at measuring point P8 under four structures.

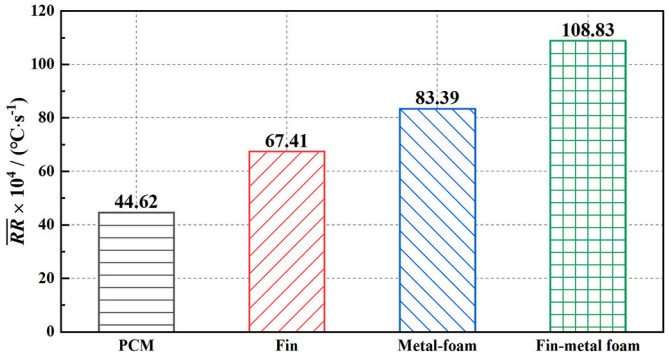

Fig. 11. Temperature response rate comparison under four structures.

factors of thermal conductivity of fins and foam, the natural convection effect of liquid paraffin is significantly weakened as described in the previous sub-section.

Comparing the overall performance of the four designs, the total melting time of pure paraffin, fin, copper foam, and the hybrid fin-foam design (as Fig. 9(a)) are 8200 s, 5900 s, 4200 s and 3000 s, respectively. Compared with the pure paraffin, taken as our benchmark case here, fin, metal foam, and the hybrid fin-foam design can reduce the melting time by 28.1%, 48.8% and 63.4%, in respective. As seen, adding fins only slightly improves the melting process compared with the benchmark case here. While fins and metal foams are both made of copper, the foam offers more uniform access for heat to be transferred to the PCM in the tank. Fins lead to a higher local liquid fraction in the vicinity of the fins but as shown before the un-finned volume of the tank, away from the fins, still transfer heat like the pure PCM. The hybrid design offered here, overcomes the "access" issue mentioned above and the foam leads to a uniform distribution of heat in the tank while fins act as low-resistance corridors to transfer heat deep into the tank away from the heated wall.

The melting time per unit mass PCM is calculated to eliminate paraffin volume changes caused by fins and copper foams, expressed as:

Table 3
Heating costs and benefits of four structures.

	PCM	FIN	MF	FMF	Unit cost
Heat storage time (h)	2.28	1.64	1.17	0.83	
Cost of PCM (yuan)	35000	35000	35000	35000	7 yuan/kg
Cost of fin (yuan)	0	76104.21	0	78457.95	18 yuan/kg
Cost of metal foam (yuan)	0	0	193299	193298.97	30000 yuan/m^3
Cost of installation (yuan)	50000	60000	60000	70000	
Initial investment (yuan)	85000.00	171104.21	288298.97	376756.92	
Operating cost (yuan)	1750.00	5555.21	11414.95	15337.85	
Annual revenue (yuan)	18439.02	25627.12	36000.00	50400.00	
Net profit (yuan)	16689.02	20071.91	24585.05	35062.15	

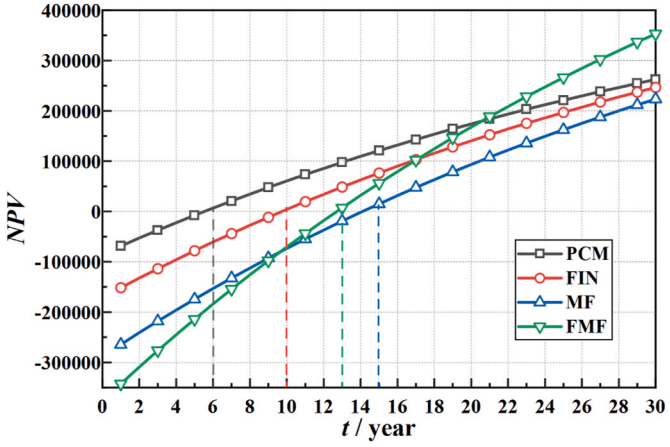

Fig. 12. Comparisons of NPV.

$$t_{mass} = \frac{t_{total}}{\rho V} \tag{2}$$

where t_{mass} and t_{total} are the melting time per unit mass PCM and melting time for the tank, ρ and V denote the density and volume for the PCM. The paraffin volumes of PCM, FIN, MF and FMF groups are 6.94×10^{-5} m^3, 6.45×10^{-5} m^3, 6.73×10^{-5} m^3 and 6.26×10^{-5} m^3, respectively. Compared to the original pure PCM, the volume of paraffin in the other three groups decreased by 7.0%, 3.0% and 9.8%, respectively. As noticed in Fig. 9(b), t_{mass} gradually decreases if fin, metal foam, and both two are inserted into the pure PCM. Compared to the original pure PCM, the other three structures reduce t_{mass} by 22.6%, 47.2%, and 59.4%, in respective. This proves that although fins and copper foams reduce part of paraffin volume, they can still achieve a positive gain in accelerating the melting process.

3.4.2. Comparison of temperature

For a fixed location, P8 (see Fig. 1), the temporal temperature variation for the four considered designs are demonstrated in Fig. 10. To ensure the same location of the points in four different structures, the point of P8 is 20 mm from the wall surface and 15 mm from the bottom plate.

As seen, different trends are observed for different designs. The temperature curve of P8 in pure PCM tank is significantly slower than that of the other three. As expected, the temperature for fin-foam hybrid PCM is higher than that of foam-PCM composite. However, interestingly, the finned tank's temperature leads to an increase in temperature among the four cases. The fin design is off to a faster start compared to the foam case but after about 2800 s, the hybrid design line crosses over. This is mainly owing to the fact that P8 is located at the fin center for the finned tank. Given the lower thermal resistance of the fin compared with the PCM, more heat is transferred to the fin than to the surrounding PCM. With the hybrid design, the fin still offers lower resistance but the foam structure near the fin has much lower resistance compared to that of the pure PCM. Hence, the heat is split between the fin and the foam leading to a slower response for the hybrid design.

To supplement the data presented in Figs. 10 and 11 is presented to compare the (P8) temperature response rate for the four designs considered here. As seen, the addition of highly conductive metal (be it foam or fin) leads to much faster response rate compared with the benchmark case. That is, compared to pure PCM, temperature response rates of fin, foam, and hybrid design increase by 51.08%, 86.89%, and 143.90%, respectively. For PCM, the three strengthening methods can significantly improve the temperature response rate, and the combination of the two methods is the most beneficial.

3.4.3. Economic analysis

In the current subsection, the economics of the four structures are analyzed in the context of a solar thermal storage system. The building area is 1000 m^2. Phase change regenerators with four structures are used to store heat for 9 h a day. The prices of materials are based on the local market. It is assumed that the weight of PCM used is 5000 kg, and other parameters are calculated according to the data in Table 3. The initial investment is the sum of PCM, fin, metal foam and installation cost. Operating expenses are assumed to be 5% of the total cost of materials. According to municipal government regulations, for the annual income, the heating period is 120 days, and the heating income is 0.25 yuan/KWH. Net profit is the difference between annual revenue minus operating costs. According to Fig. 12, the investment payback period of PCM, FIN, MF and FMF are 6, 10, 15 and 13 years respectively. In addition, we calculated the net present value (NPV) as shown in the figure below. The calculation formula is:

$$NPV = \sum_{t=0}^{n} (CI - CO)_t (1+i)^{-t} \tag{3}$$

where CI, CO, n and i represent the annual revenue, operating cost, the life cycle (assumed to be 30 years) and the discount rate (assumed to be 2.54%), in respective. As can be seen from Fig. 12, the NPV growth trend of PCM, FIN and MF groups is similar. However, the NPV trend for these three structures is PCM > FIN > MF in the life cycle due to the difference in initial investment. It should be noted that the NPV trend of FMF is significantly different from that of other structures. Although the FMF group has the maximum initial investment, its profit growth rate is the fastest. The main reason is that the PCM melting time in the FMF is drastically shortened. Therefore, the energy storage efficiency is markedly improved. As seen, Around the 21-th years, the economic benefits of FMF surpassed those of the other three groups. Although the initial investment of FMF group is large and the payback period is long, the NPV of FMF group is the highest in the actual service life, which is a measure that can be considered in practical application.

3.5. Temperature response

3.5.1. Temperature at PCM

The temperature curves for PCM at P10 and P12 are demonstrated in Fig. 13(a) and (b). Temperature at the point is almost the same from 0 s to 500 s under five heating scenarios. And the temperature deviation

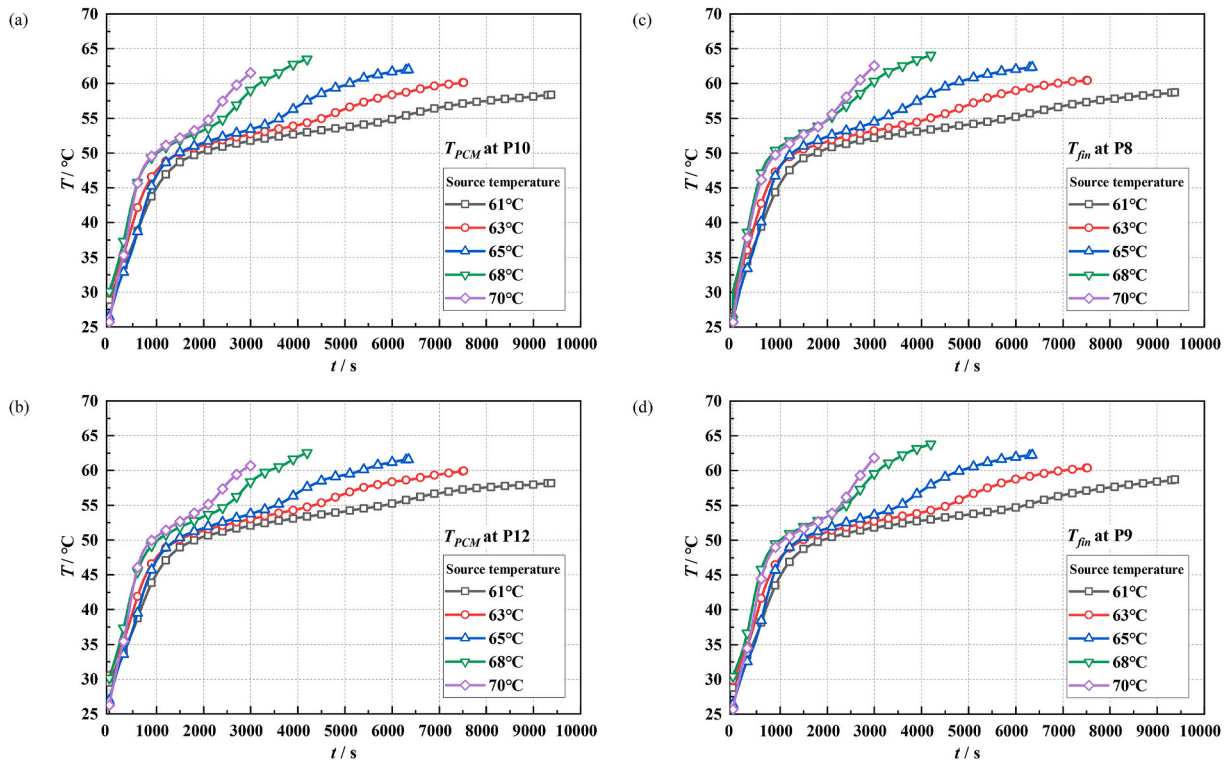

Fig. 13. Temperatures for PCM at (a) P10; or fin at (b) P8 under five heating conditions.

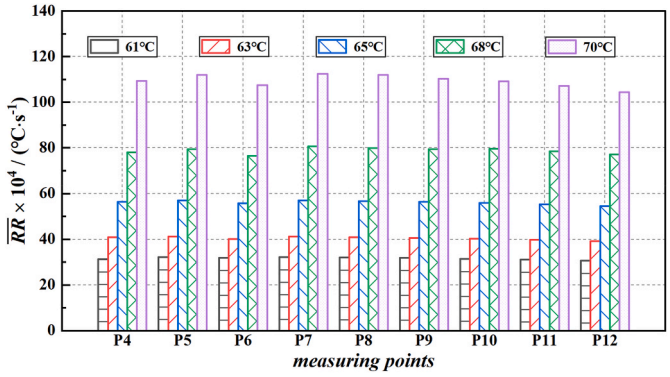

Fig. 14. Temperature comparison between fin and height direction.

starts to appear after 500 s, peaking at 3000 s. For the heating source temperatures of 61 °C and 63 °C, the PCM temperature rises in a rapid fashion before 1000 s, and the increasing ratio gradually declines, then tends to plateau. As for the other three higher source temperatures, there does not exist plateau period for temperature development. This can be understood, since the temperature difference of the five cases is not the same, which makes the temperature of the measuring point present a non-linear change trend related to the various temperature difference (driving force).

Fins are inserted into porous foam for further enhancement on thermal conduction capability. Fig. 13(c) and (d) demonstrate the temperature variation with time on two selected fin surfaces as shown in Fig. 1. The measuring points are all located at the center of the fin. P8 is located in the middle of the gravity direction, and P9 is 17 mm lower than the point. Very similar variation trend is noted for fin temperature at different locations. This indicates a better temperature uniformity that can be achieved by the fin-foam hybrid.

3.5.2. Temperature response rate comparison

To assess the temperature rise quantitatively at P8 for different cases, a quantity that describes the increasing rate for temperature is introduced here as

$$\overline{RR} = \int_0^{t_{total}} \frac{1}{t_{total}} \frac{(T_n - T_{n-1})}{(t_n - t_{n-1})} \mathrm{d}t \tag{4}$$

where $\overline{RR}$ describes the mean temperature response rate, T and t are the temperature and time, in respective; t_{total} denotes the total melting time, subscript n and $n-1$ represent the number of sequence. For the equation, according to dimensional analysis, the units of $T_n - T_{n-1}$, $t_n - t_{n-1}$ and t_{total} are °C, s and s, respectively. Therefore, the unit of $\frac{1}{t_{total}} \frac{(T_n - T_{n-1})}{(t_n - t_{n-1})} \mathrm{d}t$ is $\frac{^\circ C}{s \cdot s} \cdot s = ^\circ C/s$. Fig. 14 illustrates the temperature response rate at nine measuring points (Fig. 1 depicts the measurement points P4–P12) for five different heat source temperature values. As increasing heat source temperature, the temperature response rate of all measuring points grows in a rapid fashion. Using the heat source temperature of 61 °C as the benchmark, the average temperature of measuring points increases the temperature response rate by 27.95%, 60.53%, 84.20% and 98.62% respectively. Besides, the average temperature response rates at P7, P8 and P9 are highest compared to other points since they are located at the fin surface. However, the difference is not significant, indicating a better temperature uniformity that can be achieved by the fin-foam hybrid.

4. Conclusions

This paper reports the melting process of the composite phase change material in copper foam, fins, and hybrid of them at different temperatures. The phase interface changes and the real-time temperature response of each measuring point at different temperatures are recorded, with discussing the influence of different heat source temperatures on the melting process. Four structures (pure paraffin, fin, metal foam, and fin-metal foam hybrid) are compared to verify the strengthening effect of the hybrid structure.

Following conclusions are drawn:

(1) The melting rate of the phase interface at the fin is faster than that far away from it, causing an uneven shape for the phase interface. Natural convection plays a dominating role in forming phase interface in pure PCM and PCM-foam scenarios. With fin inserted, heat conduction contributes more profoundly to melting.
(2) The increase in heat source temperature markedly reduces the complete melting time. 70 °C heating can save 67.7% of melting time compared to the 61 °C heating. For every 1 °C increase in the heat source temperature from 61 °C to 70 °C, the complete melting time decreases by 700 s on average.
(3) Compared with pure PCM, the complete melting time of fin-metal foam hybrid is reduced by 63.4% and the temperature response rate is increased by 146.44%. This reveals the competing solution to improving the melting process.
(4) A more uniform temperature distribution is achieved by the hybrid, compared to the segment structure.

Declaration of competing interest

The authors declare that they have no known competing financial interests or personal relationships that could have appeared to influence the work reported in this paper.

Data availability

Data will be made available on request.

Acknowledgement

This work was supported by the the National Key R&D Program of China (2018YFD1100201), the National Natural Science Foundation of China (51976155). The author (Xiaohu Yang) gratefully acknowledged the support of K. C. Wong Education Foundation.

References

[1] E. Kabir, P. Kumar, S. Kumar, A.A. Adelodun, K.-H. Kim, Solar energy: potential and future prospects, Renew. Sustain. Energy Rev. 82 (2018) 894–900.
[2] H. Mahon, D. O'Connor, D. Friedrich, B. Hughes, A review of thermal energy storage technologies for seasonal loops, Energy 239 (2022), 122207.
[3] R. Baby, C. Balaji, Thermal performance of a PCM heat sink under different heat loads: an experimental study, Int. J. Therm. Sci. 79 (2014) 240–249.
[4] R. Akula, C. Balaji, Thermal performance of a phase change material-based heat sink subject to constant and power surge heat loads: a numerical study, J. Therm. Sci. Eng. Appl. 13 (2020).
[5] A. Abdulla, K.S. Reddy, Effect of operating parameters on thermal performance of molten salt packed-bed thermocline thermal energy storage system for concentrating solar power plants, Int. J. Therm. Sci. 121 (2017) 30–44.
[6] S. Khanna, K.S. Reddy, T.K. Mallick, Optimization of finned solar photovoltaic phase change material (finned pv pcm) system, Int. J. Therm. Sci. 130 (2018) 313–322.
[7] A.K. Raj, M. Srinivas, S. Jayaraj, CFD modeling of macro-encapsulated latent heat storage system used for solar heating applications, Int. J. Therm. Sci. 139 (2019) 88–104.
[8] B. Xie, C. Li, B. Zhang, L. Yang, G. Xiao, J. Chen, Evaluation of stearic acid/coconut shell charcoal composite phase change thermal energy storage materials for tankless solar water heater, Energy Built Environ. 1 (2020) 187–198.
[9] Y. Rghif, B. Zeghmati, F. Bahraoui, Modeling the influences of a phase change material and the Dufour effect on thermal performance of a salt gradient solar pond, Int. J. Therm. Sci. 166 (2021), 106979.
[10] C. Shen, G. Lv, K. Zheng, C. Ruan, C. Zhang, Y. Dong, Modeling and investigating the detailed characteristics of solar lighting/heating system based on spectrum split of nanofluids, Energy Built Environ. 3 (2022) 30–39.
[11] H. Li, Z. Wang, T. Hong, M.A. Piette, Energy flexibility of residential buildings: a systematic review of characterization and quantification methods and applications, Adv. Appl. Energy 3 (2021), 100054.
[12] P.W. Griffin, G.P. Hammond, R.C. McKenna, Industrial energy use and decarbonisation in the glass sector: a UK perspective, Adv. Appl. Energy 3 (2021), 100037.
[13] M. Alizadeh, M.H. Pahlavanian, M. Tohidi, D.D. Ganji, Solidification expedition of Phase Change Material in a triplex-tube storage unit via novel fins and SWCNT nanoparticles, J. Energy Storage 28 (2020), 101188.
[14] M. Hassani Soukht Abandani, D. Domiri Ganji, Melting effect in triplex-tube thermal energy storage system using multiple PCMs-porous metal foam combination, J. Energy Storage 43 (2021), 103154.
[15] J. Guo, Z. Liu, B. Yang, X. Yang, J. Yan, Melting assessment on the angled fin design for a novel latent heat thermal energy storage tube, Renew. Energy 183 (2022) 406–422.
[16] J. Guo, X. Wang, B. Yang, X. Yang, M.-J. Li, Thermal assessment on solid-liquid energy storage tube packed with non-uniform angled fins, Sol. Energy Mater. Sol. Cell. 236 (2022), 111526.
[17] N. Zhang, Y. Yuan, Synthesis and thermal properties of nanoencapsulation of paraffin as phase change material for latent heat thermal energy storage, Energy Built Environ. 1 (2020) 410–416.
[18] A.K. Pandey, M. George, N.A. Rahim, V.V. Tyagi, S. Shahabuddin, R. Saidur, Preparation, characterization and thermophysical properties investigation of A70/polyaniline nanocomposite phase change material for medium temperature solar applications, Energy Built Environ. 2 (2021) 271–277.
[19] K-i Tanoue, M. Nagao, A. Yoshida, T. Nishimura, Heat transfer and phase change in a polystyrene packed bed during melting, Int. J. Heat Mass Tran. 79 (2014) 324–331.
[20] Z. Duan, Z. Zhang, J. Wang, X. Cao, J. Zhang, Thermal performance of structured packed bed with encapsulated phase change materials, Int. J. Heat Mass Tran. 158 (2020), 120066.
[21] T. Xiao, X. Yang, K. Hooman, T.J. Lu, Analytical fractal models for permeability and conductivity of open-cell metallic foams, Int. J. Heat Mass Tran. 177 (2021), 121509.
[22] C. Zhao, M. Opolot, M. Liu, F. Bruno, S. Mancin, R. Flewell-Smith, et al., Simulations of melting performance enhancement for a PCM embedded in metal periodic structures, Int. J. Heat Mass Tran. 168 (2021), 120853.
[23] C. Zhao, M. Opolot, M. Liu, F. Bruno, S. Mancin, K. Hooman, Phase change behaviour study of PCM tanks partially filled with graphite foam, Appl. Therm. Eng. 196 (2021), 117313.
[24] T. Xiao, X. Yang, K. Hooman, L. Jin, C. Yang, T.J. Lu, Conductivity and permeability of graphite foams: Analytical modelling andpore-scale simulation, Int. J. Therm. Sci. 179 (2022), 107706.
[25] S. Tiari, S. Qiu, Three-dimensional simulation of high temperature latent heat thermal energy storage system assisted by finned heat pipes, Energy Convers. Manag. 105 (2015) 260–271.
[26] K. Gopi Kannan, R. Kamatchi, Experimental investigation on thermosyphon aid phase change material heat exchanger for electronic cooling applications, J. Energy Storage 39 (2021), 102649.
[27] P. Zhang, Z.N. Meng, H. Zhu, Y.L. Wang, S.P. Peng, Melting heat transfer characteristics of a composite phase change material fabricated by paraffin and metal foam, Appl. Energy 185 (2017) 1971–1983.
[28] R. Baby, C. Balaji, Experimental investigations on thermal performance enhancement and effect of orientation on porous matrix filled PCM based heat sink, Int. Commun. Heat Mass Tran. 46 (2013) 27–30.
[29] X. Hu, F. Zhu, X. Gong, Experimental and numerical study on the thermal behavior of phase change material infiltrated in low porosity metal foam, J. Energy Storage 26 (2019), 101005.
[30] X. Huang, C. Sun, Z. Chen, Y. Han, Experimental and numerical studies on melting process of phase change materials (PCMs) embedded in open-cells metal foams, Int. J. Therm. Sci. 170 (2021), 107151.
[31] M. Al-Jethelah, S. Ebadi, K. Venkateshwar, S.H. Tasnim, S. Mahmud, A. Dutta, Charging nanoparticle enhanced bio-based PCM in open cell metallic foams: an experimental investigation, Appl. Therm. Eng. 148 (2019) 1029–1042.
[32] G.K. Marri, C. Balaji, Experimental and numerical investigations on the effect of porosity and PPI gradients of metal foams on the thermal performance of a composite phase change material heat sink, Int. J. Heat Mass Tran. 164 (2021), 120454.
[33] H. Li, C. Hu, Y. He, D. Tang, K. Wang, X. Hu, Visualized-experimental investigation on the energy storage performance of PCM infiltrated in the metal foam with varying pore densities, Energy 237 (2021), 121540.
[34] E.I. Mohamed Moussa, M. Karkri, A numerical investigation of the effects of metal foam characteristics and heating/cooling conditions on the phase change kinetic of phase change materials embedded in metal foam, J. Energy Storage 26 (2019), 100985.
[35] V. Joshi, M.K. Rathod, Thermal performance augmentation of metal foam infused phase change material using a partial filling strategy: an evaluation for fill height ratio and porosity, Appl. Energy 253 (2019), 113621.
[36] B. Buonomo, H. Celik, D. Ercole, O. Manca, M. Mobedi, Numerical study on latent thermal energy storage systems with aluminum foam in local thermal equilibrium, Appl. Therm. Eng. 159 (2019), 113980.
[37] J. Guo, Z. Du, G. Liu, X. Yang, M.-J. Li, Compression effect of metal foam on melting phase change in a shell-and-tube unit, Appl. Therm. Eng. (2022), 118124.
[38] P. Poureslami, M. Siavashi, H. Moghimi, M. Hosseini, Pore-scale convection-conduction heat transfer and fluid flow in open-cell metal foams: a three-dimensional multiple-relaxation time lattice Boltzmann (MRT-LBM) solution, Int. Commun. Heat Mass Tran. 126 (2021), 105465.
[39] Q. Han, H. Wang, C. Yu, C. Zhang, Lattice Boltzmann simulation of melting heat transfer in a composite phase change material, Appl. Therm. Eng. 176 (2020), 115423.
[40] G. Wang, G. Wei, C. Xu, X. Ju, Y. Yang, X. Du, Numerical simulation of effective thermal conductivity and pore-scale melting process of PCMs in foam metals, Appl. Therm. Eng. 147 (2019) 464–472.

[41] S. Abishek, A.J.C. King, N. Nadim, B.J. Mullins, Effect of microstructure on melting in metal-foam/paraffin composite phase change materials, Int. J. Heat Mass Tran. 127 (2018) 135–144.
[42] R. Sabrina Ferfera, B. Madani, R. Serhane, Investigation of heat transfer improvement at idealized microcellular scale for metal foam incorporated with paraffin, Int. J. Therm. Sci. 156 (2020), 106444.
[43] M. Gaedtke, S. Abishek, R. Mead-Hunter, A.J.C. King, B.J. Mullins, H. Nirschl, et al., Total enthalpy-based lattice Boltzmann simulations of melting in paraffin/metal foam composite phase change materials, Int. J. Heat Mass Tran. 155 (2020), 119870.
[44] Y.-L. He, Q. Liu, Q. Li, W.-Q. Tao, Lattice Boltzmann methods for single-phase and solid-liquid phase-change heat transfer in porous media: a review, Int. J. Heat Mass Tran. 129 (2019) 160–197.
[45] H. Xu, N. Wang, C. Zhang, Z. Qu, M. Cao, Optimization on the melting performance of triplex-layer PCMs in a horizontal finned shell and tube thermal energy storage unit, Appl. Therm. Eng. 176 (2020), 115409.
[46] Ç. Yıldız, M. Arıcı, S. Nižetić, A. Shahsavar, Numerical investigation of natural convection behavior of molten PCM in an enclosure having rectangular and tree-like branching fins, Energy 207 (2020), 118223.
[47] B. Fekadu, M. Assaye, Enhancement of phase change materials melting performance in a rectangular enclosure under different inclination angle of fins, Case Stud. Therm. Eng. 25 (2021), 100968.
[48] R. De Césaro Oliveski, F. Becker, L.A.O. Rocha, C. Biserni, G.E.S. Eberhardt, Design of fin structures for phase change material (PCM) melting process in rectangular cavities, J. Energy Storage 35 (2021), 102337.
[49] V. Safari, H. Abolghasemi, L. Darvishvand, B. Kamkari, Thermal performance investigation of concentric and eccentric shell and tube heat exchangers with different fin configurations containing phase change material, J. Energy Storage 37 (2021), 102458.
[50] M. Masoumpour-Samakoush, M. Miansari, S.S.M. Ajarostaghi, M. Arıcı, Impact of innovative fin combination of triangular and rectangular fins on melting process of phase change material in a cavity, J. Energy Storage 45 (2022), 103545.
[51] Y. Huang, D. Cao, D. Sun, X. Liu, Experimental and numerical studies on the heat transfer improvement of a latent heat storage unit using gradient tree-shaped fins, Int. J. Heat Mass Tran. 182 (2022), 121920.
[52] J. Wang, X. Xu, T. Sun, H. Yao, M. Song, Y. Wang, Simulation of heat storage process in spiral fin phase change heat storage unit, Energy Storage Sci. Technol. 10 (2021) 514.
[53] Z. Deng, S. Wu, H. Xu, Y. Chen, Melting heat transfer enhancement of a horizontal latent heat storage unit by fern-fractal fins, Chin. J. Chem. Eng. 28 (2020) 2857–2871.
[54] M. Opolot, C. Zhao, M. Liu, S. Mancin, F. Bruno, K. Hooman, Investigation of the effect of thermal resistance on the performance of phase change materials, Int. J. Therm. Sci. 164 (2021), 106852.
[55] J. Guo, Z. Liu, Z. Du, J. Yu, X. Yang, J. Yan, Effect of fin-metal foam structure on thermal energy storage: an experimental study, Renew. Energy 172 (2021) 57–70.
[56] M. Arıcı, E. Tütüncü, Ç. Yıldız, D. Li, Enhancement of PCM melting rate via internal fin and nanoparticles, Int. J. Heat Mass Tran. 156 (2020), 119845.
[57] X. Yang, J. Yu, T. Xiao, Z. Hu, Y.-L. He, Design and operating evaluation of a finned shell-and-tube thermal energy storage unit filled with metal foam, Appl. Energy 261 (2020), 114385.
[58] C. Ding, L. Wang, Z. Niu, Thermal performance evaluation of latent heat storage systems with plate fin-metal foam hybrid structure, Case Stud. Therm. Eng. 27 (2021), 101309.
[59] X. Yang, P. Wei, G. Liu, Q. Bai, Y.-L. He, Performance evaluation on the gradient design of pore parameters for metal foam and pin fin-metal foam hybrid structure, Appl. Therm. Eng. 175 (2020), 115416.
[60] C. Ding, Y. Shan, Q. Nie, Thermal performance of phase change material–based heat sink with hybrid fin–metal foam structure under hypergravity conditions, Int. J. Energy Res. 46 (2022) 5811–5827.
[61] X. Meng, L. Meng, J. Zou, F. He, Influence of the copper foam fin (CFF) shapes on thermal performance of phase-change material (PCM) in an enclosed cavity, Case Stud. Therm. Eng. 23 (2021), 100810.
[62] P. Jany, A. Bejan, Scaling theory of melting with natural convection in an enclosure, Int. J. Heat Mass Tran. 31 (1988) 1221–1235.